DOI:10.11858/gywlxb.20261154

Pressure-Induced Dome-Shaped Superconductivity in Topological Dirac Semimetal KZnBi*

ZHENG Qunfei[1], ZHAO Lingxiao[1,2], TONG Haoxuan[1], CHENG Wenjing[1], LI Chenkai[1], LIU Jingyi[1], CHEN Wuhao[2], LIU Ying[2,3], ZHU Jinlong[1, 2, 3*]

(1. Department of Physics, State Key Laboratory of Quantum Functional Materials, Guangdong Basic Research Center of Excellence for Quantum Science, Southern University of Science and Technology (SUSTech), Shenzhen 518055, Guangdong, China;
2. Quantum Science Center of Guangdong-Hong Kong-Macao Greater Bay Area (Guangdong), Shenzhen 518045, Guangdong, China;
3. Institute of Major Scientific Facilities for New Materials, Southern University of Science and Technology, Shenzhen 518055, Guangdong, China)

Abstract: The three-dimensional topological Dirac semimetal KZnBi hosts symmetry-protected Dirac fermions and exhibits superconductivity, providing an attractive system for studying the interplay between topological states and superconductivity. We report high-pressure measurements of the temperature-dependent resistance, transverse magnetoresistance, and Hall resistance of KZnBi up to 36 GPa. The superconducting transition temperature T_c^{onset} shows a nonmonotonic

**Received date: 2026-08-27; Revised date: 2026-10-10
Foundation item: National Natural Science Foundation of China (12461160274, 12274193, 12304223); Shenzhen Science and Technology Program (JCYJ20230807093301003); Guangdong Provincial Quantum Science Strategic Initiative (GDZX2201001); Guangdong Basic and Applied Basic Research Foundation (2022A1515010044)
First author: ZHENG Qunfei (1996–), female, Ph.D. student, mainly engaged in research on high-pressure tuning of topological insulators. E-mail: 12131280@mail.sustech.edu.cn
ZHAO Lingxiao, mainly engaged in research on high-pressure tuning of topological insulators. E-mail: zhaolingxiao@quantumsc.cn
Corresponding author: ZHU Jinlong (1981–), male, Ph.D., associate professor, mainly engaged in research on quantum control of condensed matter under high pressure, high-energy matter systems induced by high-pressure in situ laser heating and their novel physical properties, high-pressure synthesis and neutron characterization of natural gas hydrates, and crystal-field design of solid-state electrolytes and interfacial studies of energy storage devices. E-mail: zhujl@sustech.edu.cn

录用录用，非最终出版稿

pressure dependence. The first dome begins to form at around 0.9 GPa, with T_c^{onset} reaching its maximum at about 1.6 GPa before decreasing to a minimum near 4.0 GPa. Upon further compression, T_c^{onset} rises again and forms a second dome with a maximum of approximately 4.2 K at 15.8 GPa. These results establish a rich temperature–pressure phase diagram for KZnBi and demonstrate a close connection between its superconducting behavior and the electronic structure.

Keywords: high pressure; topological dirac semimetal; superconductivity; superconducting transition temperature; Hall resistance
CLC number: O521.2 Document code: A

Three-dimensional topological Dirac semimetals possess symmetry-protected bulk Dirac points and serve as a versatile platform for exploring exotic quantum phases. Through breaking time-reversal or inversion symmetry, they can be driven into other topological states such as Weyl semimetals, and may further host or induce topological superconductivity.[1–8] Among various material candidates, ternary ABC compounds with planar honeycomb structures (where A = alkali/alkaline-earth metal, B = transition metal, C = pnictogen/chalcogen element) offer a highly tunable platform for topological states. This tunability stems from their versatile chemical compositions, which allow for the engineering of electronic structures and spin–orbit coupling strength.[9–12] Examples range from hourglass fermions in KHgSb[13,14] to topological Dirac and Weyl semimetals such as KZnBi, BaAgBi, SrCuBi, and CaAuAs.[15-18] Notably, several members of this family are superconducting at ambient pressure, such as KZnBi at 0.85 K, SrCuBi at 2.1 K, BaAgBi at 3.8 K, and SrPtAs at 2.4 K.[15,17,19] KZnBi is a prototypical 3D topological Dirac semimetal, in which Dirac points along the Γ–A line protected by inversion and threefold rotational symmetries. Intriguingly, it displays surface superconductivity below 0.85 K on the (001) surface while the bulk remains non-superconducting at ambient pressure,[15] making it an ideal system to study topological superconductivity.

Pressure offers a clean and powerful means to continuously tune the lattice and electronic structures of quantum materials without introducing chemical disorder. In layered systems, pressure can effectively modify interlayer coupling and electronic dimensionality, thereby driving novel phase transitions. For instance, $SrAs_3$ undergoes a pressure-induced transition from a nodal-line semimetal to a topological crystalline insulator. This structural evolution enhances three-dimensional electronic coupling and leads to the emergence of superconductivity with T_c ~ 5.8 K.[20] In $NbIrTe_4$, applied pressure strengthens the interlayer Te–Te bonding, shifting the electronic structure from a multiband to a hole-dominated character, and eventually gives rise to superconductivity above ~39 GPa.[21] Similarly, compressed Cd_3As_2 develops SC (T_c = 2.0 – 4.0 K) with an anomalous plateau between 21.3 – 50.9 GPa.[22] These findings highlight pressure as a unique means to explore and potentially enhance superconducting states in topological materials. Among various layered topological systems, KZnBi possesses both three-dimensional Dirac states and surface superconductivity, yet its behavior under pressure remains unexplored. The observation of significantly enhanced superconductivity under pressure in the isostructural compound SrCuBi[19] raises the question of whether a similar enhancement can occur in KZnBi, and what electronic

录用稿件，非最终出版稿

mechanisms underlie such behavior. However, a key structural difference between KZnBi and SrCuBi is the interlayer cation, K^+ in KZnBi versus Sr^{2+} in SrCuBi, whose larger ionic radius leads to weaker interlayer coupling and a longer *c*-axis in KZnBi, potentially causing distinct pressure responses.

Here, we present a comprehensive high-pressure study of the topological Dirac semimetal KZnBi through measurements of temperature-dependent resistance, transverse magnetoresistance, and Hall resistance. Our work maps the superconducting phase diagram up to 36 GPa and reveals a double dome like behavior in the pressure dependence of the transition temperature. The suppression of the first superconducting dome coincides with distinct anomalies in carrier concentration and mobility around 4 GPa, indicating a likely pressure-induced electronic reconstruction. The second dome shows a maximum transition temperature $T_c^{\mathrm{onset}} \approx$ 4.2 K near 15.8 GPa. This work illustrates how electron correlations and superconducting order evolve concurrently in KZnBi under pressure.

1. Experimental Methods

KZnBi single crystals were synthesized via the Bridgman method. Stoichiometric amounts of raw materials were sealed within an evacuated quartz tube containing a corundum crucible. The assembly was heated to 600 ℃ for 20 hours, slowly cooled to 300 ℃ over several hours, and finally quenched in water.[15] The crystal structure was characterized by X-ray diffraction (XRD, performed on a Rigaku SmartLab diffractometer using Cu Kα radiation) at room temperature. Raman spectra were acquired in backscattering geometry utilizing a SpectraPro HRS-500 spectrometer equipped with a liquid-nitrogen-cooled CCD detector, employing a 532 nm laser (2.84 mW power, 3.0 μm focused spot diameter) and a 1200 g·mm^{-1} grating. The chemical composition was analyzed using a JEOL JSM-7610F Plus scanning electron microscope equipped with energy-dispersive X-ray spectroscopy (EDS).

Ambient-pressure transport measurements below 2 K were carried out using a dilution refrigerator option integrated in the DynaCool system. Electrical transport measurements under high pressure and low temperatures (2–300 K) were conducted in a multifunctional measurement system. This system integrated a 14 T superconducting magnet (Cryomagnetics C-Mag), a precision current source (Keithley, 6221), and a nanovoltmeter (Keithley 2182A). Pressure was generated using a nonmagnetic diamond anvil cell fabricated from beryllium-copper alloy. Diamond anvils with 300 μm culet diameters were employed. A pre-indented CuBe gasket with initial thickness of ~30 μm was prepared. A 150 μm diameter hole was laser-drilled at the gasket center to form a sample chamber. Electrical insulation between the gasket and electrodes was achieved by filling the chamber with a composite of epoxy resin and cubic boron nitride powder (weight ratio of 1:4). After curing, a 100 μm diameter cavity was drilled in the insulating layer. NaCl served as the pressure-transmitting medium. Four gold foil electrodes were manually arranged on the insulating layer, with leads extending into the sample chamber to ensure Ohmic contact. Pressure calibration at room temperature utilized the ruby fluorescence method, monitoring the R_1 peak shift of ruby spheres co-loaded in the chamber.[23] Due to the high reactivity of KZnBi under ambient conditions, all sample preparation and handling were performed in recirculating glove boxes filled with high-purity argon gas (99.999%) to prevent aging and oxidation.

录用稿件，非最终出版稿

2. Results and Discussion

KZnBi crystallizes in the nonsymmorphic space group $P6_3/mmc$ at ambient conditions [Fig. 1(a)]. Its structure consists of alternating anionic $[ZnBi]^-$ honeycomb layers and K^+ layers stacked along the *c*-axis, exhibiting inversion symmetry centered on K ions and threefold rotational symmetry within the honeycomb planes. Single-crystal XRD patterns show only (00*l*) reflection peaks [Fig. 1(b)], consistent with previous reports.[15] EDS analysis yields a K: Zn: Bi atomic ratio of approximately 1:1:1 within experimental error [Fig. 1(c)]. Electrical transport measurements exhibit superconductivity with an onset transition temperature T_c^{onset} of ~0.83 K at ambient pressure [Fig. 1(d)], in agreement with the literature.[15] Trace amounts of elemental Bi are detected by Raman spectroscopy through characteristic modes near 70 and 96 cm^{-1} (see Appendix Fig. S1).[24] The absence of diffraction peaks from elemental Bi in XRD indicates that its concentration is below the detection limit of that technique. Hall effect measurements at 1.8 K confirm *n*-type carrier conduction in KZnBi single crystals (see Appendix Fig. S2), with a carrier density $n_e \sim 10^{18}$ cm^{-3} derived from the Hall coefficient.

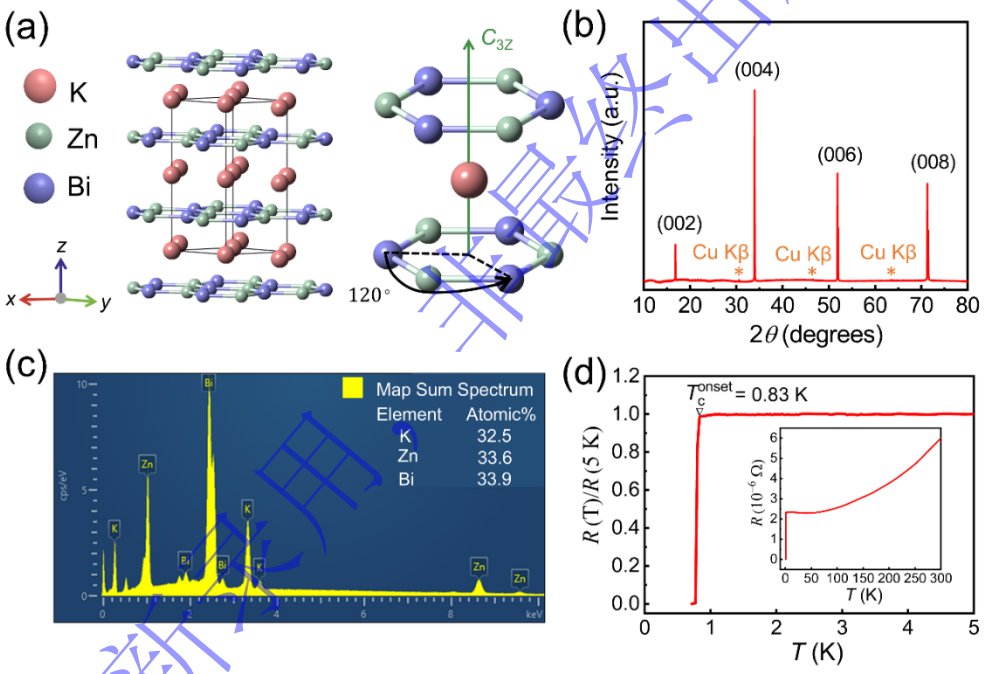


FIG. 1. (a) The crystal structure of KZnBi (space group $P6_3/mmc$) consists of ZnBi honeycomb layers connected by K^+ ion layers. This structure possesses C_{3z} rotation symmetry and inversion symmetry. (b) Single-crystal XRD patterns of the (00*l*) peaks for KZnBi. The orange asterisk indicates a set of systematic diffraction signals arising from incompletely filtered Cu Kβ radiation (λ = 1.3922 Å). (c) Energy dispersive x-ray spectroscopy of single crystal KZnBi. (d) Temperature dependence of the in-plane resistance below 5 K. Inset, temperature dependence of the in-plane resistance from 0.7 K to 300 K.

Figures 2(a) and 2(b) show the temperature-dependent resistance $R(T)$ of KZnBi under pressures up to 36.0 GPa. The onset superconducting transition temperature T_c^{onset}, defined as the intersection of linear extrapolations from the normal and superconducting regions, exhibits a non-monotonic

evolution. At ambient pressure, T_c^{onset} is ~0.83 K. Upon compression to 0.9 GPa, T_c^{onset} increases to ~3.0 K. With further pressure increase, T_c^{onset} rises to ~3.2 K at 1.6 GPa, then decreases to a minimum around 4.0 GPa, suggesting a possible electronic reconstruction above this pressure. Above 4.0 GPa, T_c^{onset} rises again, forming a dome that peaks at ~4.2 K around 15.8 GPa before decreasing at higher pressures. To determine the superconducting transition width at several representative pressures, the same criterion is used: $\Delta T_{\text{onset}-90\%} = T_c^{\text{onset}} - T_c^{90\%R_N}$, where R_N is the normal-state resistance above T_c. The transition widths are 0.86 K at 0.9 GPa, 0.755 K at 1.6 GPa, 0.547 K at 4.0 GPa, and 0.41 K at 15.8 GPa. These values remain in the range 0.4–0.9 K, showing no significant pressure-induced broadening, and are much smaller than the total variation of T_c^{onset} over the investigated pressure range. The solid pressure-transmitting medium NaCl used in this study has an ideal hydrostatic limit of about 1 GPa at room temperature, and as a solid medium it develops deviatoric/shear stresses at higher pressures, which may affect the connectivity of the superconducting phase and macroscopic phase coherence. In the layered superconductor $La_4Ni_3O_{10-\delta}$, bulk superconductivity and zero resistance are achieved when helium is used as the pressure-transmitting medium, whereas with KBr only a diamagnetic response is observed and zero resistance is never reached, indicating that non-hydrostatic pressure disrupts the uniformity of the superconducting phase and suppresses macroscopic phase coherence.[25] This comparison suggests that a zero-resistance state might be observed in KZnBi if a pressure-transmitting medium with better hydrostaticity were employed. The high-pressure behavior of KZnBi is consistent with reports on materials such as SrCuBi, where a zero-resistance state is also achieved only at significantly higher pressures, despite showing signatures of superconductivity at ambient pressure.[19]

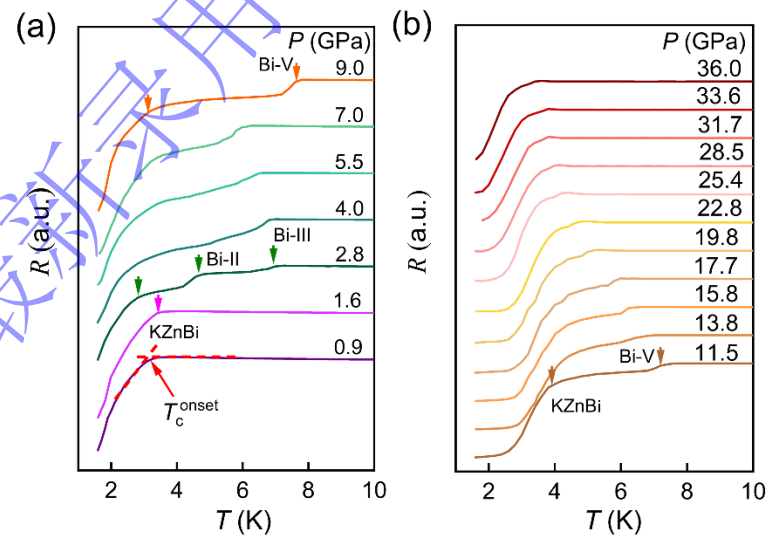


FIG. 2. Low-temperature *R*(T) curves of KZnBi under pressure. Solid triangle denotes the T_c^{onset} at their respective pressures. All the curves are offset for clarity (see the original data in Appendix Fig. S3).

最终录用，非最终出版稿

We note that additional superconducting transitions appear at 2.8 GPa [Fig. 2(a)], with onset temperatures near 4.7 K and 7.0 K. These correspond to the critical temperatures of elemental bismuth phases Bi-II ($T_c^{\text{onset}} \approx 3.9$ K at ~2.5 GPa) and Bi-III ($T_c^{\text{onset}} \approx 7$ K at ~2.8 GPa). At 9.0 GPa, the Bi-V phase emerges with $T_c^{\text{onset}} \approx 7.7$ K;[26,27] the temperature-pressure phase diagram of elemental Bi is summarized in Appendix Fig. S4. Although Bi impurities are detected by Raman spectroscopy and transport, the dominant electronic response originates from the KZnBi phase. The possibility that Bi micro-filaments form parallel conducting channels cannot be fully excluded. If Bi micro-filaments formed continuous low-resistance or superconducting paths, the overall resistance would be significantly reduced, possibly even reaching zero. However, the resistivity of KZnBi remains over 15 times larger than that of pure Bi at 0.9 GPa and about 70 times larger at 13.8 GPa (Appendix Fig. S5)., and no zero-resistance state is observed. These observations indicate that the Bi impurities most likely do not form continuous conducting channels and therefore do not dominate transport, with the KZnBi matrix remaining the main conduction path.

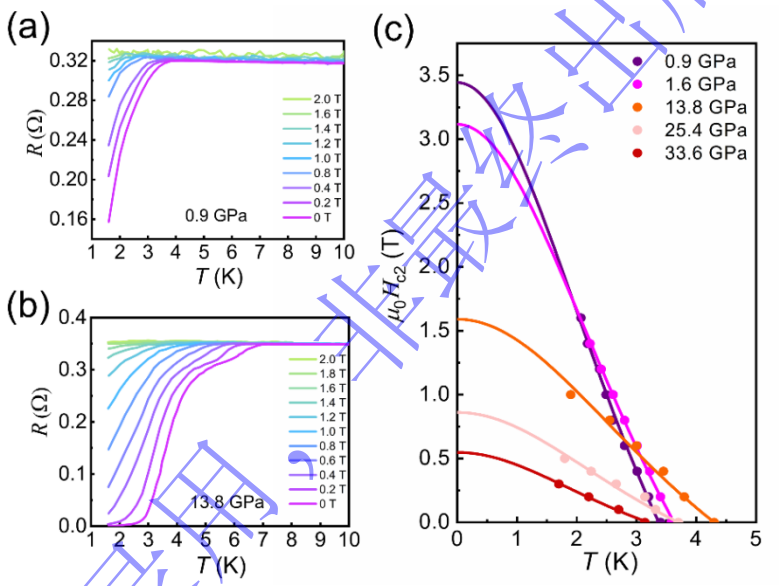


FIG. 3. (a–b) Field dependences of electrical resistance for KZnBi at 0.9 GPa (a) and 13.8 GPa (b). (c) Upper critical fields extracted from (a-b) and Fig. S5 using the T_c^{onset} criterion. Ginzburg–Landau fitting of the upper critical fields at 0.9 GPa, 1.6 GPa, 13.8 GPa, 25.4 GPa and 33.6 GPa, respectively. The solid lines represent the G-L model fitting curves, with *B* perpendicular to the current plane.

Figures 3(a) and 3(b) present the field-dependent magnetoresistance with *B* perpendicular to the current plane at 0.9 GPa and 13.8 GPa. The $\mu_0 H_{c2}$(T) data at additional pressures are provided in Appendix Fig. S6. The progressive suppression of superconductivity under magnetic fields confirms the resistive transition is attributed to superconductivity. The upper critical field $\mu_0 H_{c2}$(T) is well described by the Ginzburg-Landau (G-L) expression $\mu_0 H_{c2}(T) = \mu_0 H_{c2}(0) [\frac{1-t^2}{1+t^2}]$, where $t=T/T_c$,[28] as shown by the solid lines in Fig. 3(c). The extracted $\mu_0 H_{c2}(0)$ values decrease from 3.4 T at 0.9 GPa to 0.5 T at 33.6 GPa. The corresponding Pauli paramagnetic limit[29] $\mu_0 H_p = 1.84 T_c$ decreases from ~5.5 T at 0.9 GPa to ~3.7 T at 33.6 GPa. Since all $\mu_0 H_{c2}(0)$ values lie well below these limits,

最终录用 非最终出版稿

significant Pauli-limiting effects can be ruled out. The superconducting coherence length $\xi_{GL}(0)$, calculated from $\mu_0 H_{c2}(0) = \Phi_0/(2\pi\xi^2_{GL}(0))$ (where $\Phi_0 = 2.07\times10^{-15}$ Wb is the flux quantum), increased from 9.8 nm to 25.7 nm with increasing pressure.

To unravel the electronic origin of the superconducting evolution, we performed systematic magnetotransport and Hall measurements under pressure. Figure 4 presents the pressure dependence of $MR = (R(B) - R(0))/R(0)\times100\%$ and Hall resistance $R_{xy}(H)$ at 10 K. The MR value at 9 T increases from 14.1% at 0.9 GPa to about 26% in the pressure range of 4.0–7.0 GPa, followed by a pronounced suppression above 9.0 GPa and eventually drops below 10% at 17.3 GPa. Such suppression resembles the behavior observed in high-mobility semimetals, where the reduction of carrier mobility dominates the MR decrease.[30,31] Consistently, our Hall measurements reveal a systematic evolution of carrier parameters, as discussed below. At 0.9 GPa, the MR exhibits a quadratic field dependence (H^2) at low fields ($H < H^*$) and crosses over to a linear regime above $H^* \approx 3.8$ T. At 4.0 GPa, a similar crossover occurs at a lower field, $H^* \approx 3$ T. This field-induced crossover is reminiscent of the behavior of KZnBi at ambient pressure, where the magnetoresistance enters a quantum limit regime and shows linear growth at sufficiently high magnetic fields.[15,32] Thus, the linear positive MR under high pressure likely stems from the same mechanism, i.e., the system entering the quantum-limited state.[33-35]

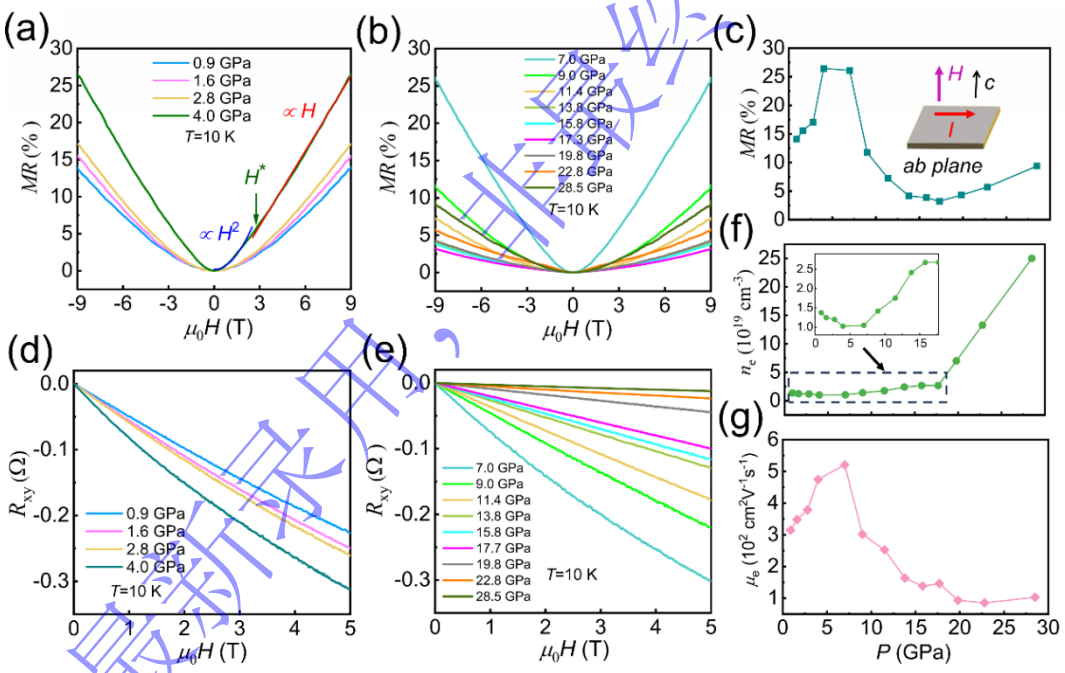


FIG. 4. Field dependence of the transverse magnetoresistance $MR = \frac{R(B)-R(0)}{R(0)} \times 100\%$ and the Hall resistance R_{xy} under pressure. (a, b) MR at 10 K under different pressures with the magnetic field applied along the c-axis (perpendicular to the current plane). The MR exhibits a quadratic field dependence ($MR \propto H^2$) in the low-field region and a linear field dependence beyond the critical field H^*. (c) Pressure dependence of the MR. The inset shows a schematic of the applied current direction, the natural cleavage plane of the sample, and the direction of the applied magnetic field. (d, e) Pressure dependence of the R_{xy} at 10 K with the magnetic field applied along the c-axis (perpendicular to the current plane). (f) Carrier concentration n_e as a function of pressure at 10 K. The inset

录用稿件，非最终出版稿

shows a zoomed-in view of the carrier concentration in the 0.9 – 17.3 GPa range. (g) Pressure dependence of the μ_e at 10 K.

Figures 4(d) and 4(e) display the evolution of $R_{xy}(H)$ with pressure. The Hall slope remains negative at 0.9 GPa, indicating dominant electron-type carriers. The absolute value of the Hall slope increases monotonically up to 4.0 GPa, implying decreasing carrier density. Above 7.0 GPa, the slope magnitude gradually diminishes. From the Hall coefficient $R_H = dR_{xy}/dH$, the carrier concentration $n_e = -1/(eR_H)$ first decreases below 4 GPa and then increases monotonically above 5 GPa [Fig. 4(f)]. Specifically, n_e rises significantly from about 1.3×10^{19} cm^{-3} at 0.9 GPa to approximately 2.5×10^{20} cm^{-3} at 28.5 GPa, representing an enhancement of nearly one order of magnitude. The mobility μ_e is 314.5 cm$^2\cdot$V$^{-1}\cdot$s^{-1} at 0.9 GPa and reaches a maximum of about 500 cm$^2\cdot$V$^{-1}\cdot$s^{-1} in the pressure range of 4.0–7.0 GPa, which likely accounts for the pronounced MR enhancement in this region. Subsequently, μ_e gradually decreases beyond 9.0 GPa [Fig. 4(g)]. Notably, the pressure at which n_e starts to increase monotonically, and the pressure range where μ_e attains its maximum, coincide with the pressure range where T_c^{onset} begins to rise markedly. This correlation suggests that the increase in n_e and the optimization of μ_e reflect a favorable evolution of the electronic structure that may contribute to the enhancement of superconductivity.

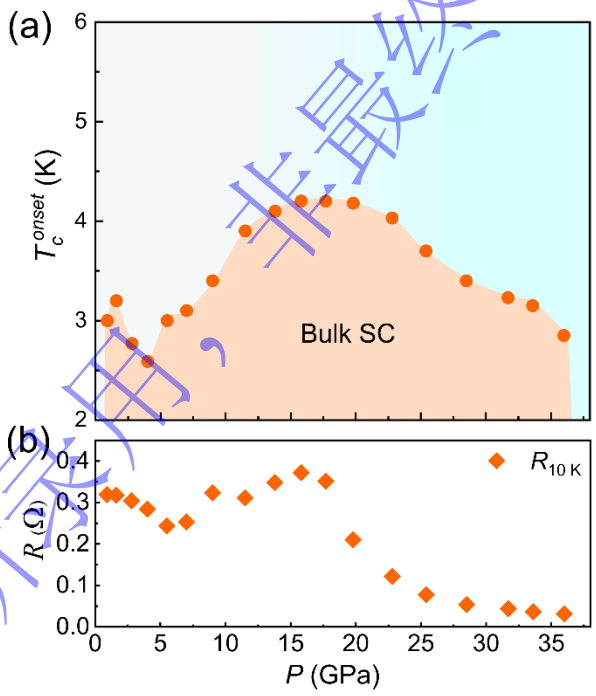


FIG. 5. (a) Temperature-pressure (*T*-*P*) phase diagram of KZnBi. (b) Pressure-dependence electrical resistance of KZnBi at 10 K.

Figure 5(a) summarizes the temperature-pressure phase diagram of KZnBi. The superconducting transition temperature T_c^{onset} increases from 0.83 K at ambient pressure to ~3.0 K at 0.9 GPa. After reaching a local maximum at P_{c1} = 1.6 GPa, it is suppressed to a minimum near 4.0 GPa. Above this pressure, T_c^{onset} rises again, forming a second dome that peaks at ~4.2 K around P_{c2} = 15.8 GPa

最新录用，非最终出版稿

before subsequently decreasing. The presence of two sequential domes suggests that the dominant factors governing superconductivity may change across different pressure regimes. To check the reliability of the phase diagram, $T_c^{90\%R_N}$ is also plotted against P, as shown in Appendix Fig. S7. The two criteria yield consistent trends: both exhibit the same two-dome structure with nearly identical characteristic pressures P_{c1} and P_{c2}. Such a pressure-tuned T_c dome is also observed in related compounds. In SrCuBi, T_c increases from 2.1 K at ambient pressure to a maximum of 4.8 K at 6.2 GPa and then decreases.[19] These comparisons may suggest that a pressure-induced T_c dome could be a common behavior in this family of topological and ABC materials, although the peak pressure and peak T_c vary with composition and structure.

The first dome at lower pressures (P < 4.0 GPa) can be qualitatively understood within a conventional BCS-like framework for a low-carrier-density superconductor, where $T_c \sim \Theta_D \exp[-1/N(0)V_0]$. Here, Θ_D is the Debye temperature, $N(0) \sim m^* n_e^{1/3}$ is the density of states at the Fermi level, m^* is the effective mass, and V_0 is the effective interaction parameter.[36,37] Hall data show that n_e decreases from 0.9 to 4.0 GPa. Consequently, the initial increase of T_c^{onset} up to $P_{c1} = 1.6$ GPa cannot be attributed to an increase in n_e. Instead, it may arise from a pressure-induced enhancement of the effective mass m^* and/or the effective pairing interaction V_0, possibly aided by an increase in Θ_D due to lattice stiffening.[38] This behavior is reminiscent of 1T-$Cu_{0.03}TiSe_2$,[39] where a dome-like T_c appears under pressure while the carrier concentration shows only weak pressure dependence, suggesting a significant change in the density of states at the Fermi level or the effective mass under pressure. The suppression of T_c^{onset} around 4.0 GPa coincides with concurrent anomalies in several key transport parameters. These include a kink in the pressure-dependent resistance at 10 K [Fig. 5(b)], as well as pronounced extrema in MR, n_e and μ_e within the 4–7 GPa range. This correlated evolution may suggest a possible connection to a pressure-induced electronic transition, such as a Fermi surface reconstruction or an electronic topological transition (ETT).[39–41] Nevertheless, transport anomalies alone are not uniquely indicative of Fermi surface reconstruction; they could also arise from other mechanisms, such as band broadening or changes in scattering processes. These anomalies are reminiscent of the high-pressure behavior of related ABC compounds. BaAgBi undergoes a structural phase transition at about 2.1 GPa,[42] while the theoretical prediction for SrCuBi suggests a pressure-induced transition from a three-dimensional topological Dirac semimetal to a trivial metal near 6–7 GPa.[19] However, whether a similar transition occurs in KZnBi near 4.0 GPa remains to be verified; in the absence of high-pressure structural data, we cannot confirm whether the lattice parameters or symmetry show any anomaly near 4.0 GPa, and consequently whether these transport anomalies can be attributed to an ETT remains an open question requiring further verification.

The suppression of T_c^{onset} is reversed above 4.0 GPa, where it begins to rise again and eventually forms a second dome. Notably, the carrier concentration n_e increases monotonically on both sides of P_{c2}=15.8 GPa, as shown in Fig. 4(f). This continuous increase in n_e across the second dome is

最新录用，非最终出版稿

difficult to reconcile with the simple BCS-like expression. To account for the dome shape within that conventional framework, one would have to invoke a pronounced, non-monotonic variation of the effective pairing interaction V with pressure, which lacks an independent microscopic justification. One possible explanation for such a dome may be provided by the theory of superconductivity with finite-range attractive interactions. Recent theoretical work by Langmann *et al*. suggested that within BCS theory, a well-defined, spatially nonlocal pairing potential can lead to a dome-shaped T_c as a function of carrier density, without requiring competing orders or quantum criticality.[43,44] In this picture, the effective pairing interaction at the Fermi surface weakens at high densities ($k_F\ell >> 1$, where κ_F is the Fermi wavevector and ℓ is the characteristic length scale of the interaction), thereby suppressing T_c. The peak in T_c^{onset} at P_{c2}=15.8 GPa may then correspond to the optimal condition where $k_F\ell \sim 1$. This scenario may be consistent with the observed second superconducting dome and raises the possibility of a unified microscopic mechanism. However, we emphasize that $k_F l$ cannot be directly obtained in the present experiments and can only be estimated for qualitative comparison. In the absence of microscopic experimental evidence for the pairing mechanism, this interpretation remains indirect and speculative, and further verification is required. Furthermore, high-pressure XRD data are currently lacking, so a structural transition near the second dome cannot be excluded, although no such transition has been reported for the sister compound SrCuBi under similar pressure.[19]

3. Conclusion

We have systematically investigated the pressure-dependent superconducting phase diagram of the three-dimensional topological Dirac semimetal KZnBi through high-pressure electrical and magnetotransport measurements. Our results reveal two distinct superconducting domes. The first dome, occurring at lower pressures, can be understood within a conventional BCS-like framework, where the superconducting transition temperature is governed by the pressure evolution of the density of states and the Debye temperature. This dome is interrupted near 4.0 GPa, likely due to a pressure-induced electronic topological transition. The second dome emerges at higher pressures and likely reflects the intrinsic non-monotonic behavior predicted for superconductivity mediated by finite-range electron-electron interactions, which becomes prominent in the high-pressure electronic phase. Future studies combining high-pressure X-ray diffraction and first-principles calculations will help clarify the structural stability and the evolution of the electronic topological state under compression.

录用稿，非最终出版稿

Acknowledgments

We thank Shenzhen Guangming Science City Development and Construction Co., Ltd. and its Material Genome Big-Science Facilities Platform, for providing technical support and assistance in data collection and analysis. Some experiments are supported by the Synergic Extreme Condition User Facility.

References

[1] Liu Z K, Zhou B, Zhang Y, et al. Discovery of a three-dimensional topological Dirac semimetal, Na_3Bi[J]. Science, 2014, 343(6172): 864-867.

[2] Liu Z K, Jiang J, Zhou B, et al. A stable three-dimensional topological Dirac semimetal Cd_3As_2[J]. Nature Materials, 2014, 13(7): 677-681.

[3] Wang Z, Sun Y, Chen X Q, et al. Dirac semimetal and topological phase transition in A_3Bi (A = Na, K, Rb) [J]. Physical Review B, 2012, 85(19): 195320.

[4] He L P, Hong X C, Dong J K, et al. Quantum transport evidence for the three-dimensional Dirac semimetal phase in Cd_3As_2[J]. Physical Review Letters, 2014, 113(24): 246402.

[5] Murakami S. Phase transition between the quantum spin Hall and insulator phases in 3D: emergence of a topological gapless phase[J]. New Journal of Physics, 2007, 9(9): 356.

[6] Huang S M, Xu S Y, Belopolski I, et al. A Weyl fermion semimetal with surface Fermi arcs in the transition metal monopnictide TaAs class[J]. Nature Communications, 2015, 6: 7373.

[7] Singh B, Sharma A, Lin H, et al. Topological electronic structure and Weyl semimetal in the $TlBiSe_2$ class of semiconductors[J]. Physical Review B, 2012, 86(11): 115208.

[8] Mardanya S, Singh B, Huang S M, et al. Prediction of threefold fermions in a nearly ideal Dirac semimetal BaAgAs[J]. Physical Review Materials, 2019, 3(7): 071201.

[9] Zhang X, Liu Q, Xu Q, et al. Topological insulators versus topological Dirac semimetals in honeycomb compounds[J]. Journal of the American Chemical Society, 2018, 140(42): 13687-13694.

[10] Zhang H J, Chadov S, Müchler L, et al. Topological insulators in ternary compounds with a honeycomb lattice[J]. Physical Review Letters, 2011, 106(15): 156402.

[11] Wang Z, Alexandradinata A, Cava R J, et al. Hourglass fermions[J]. Nature, 2016, 532(7598): 189-194.

[12] Gao H, Kim Y, Venderbos J W F, et al. Dirac–Weyl semimetal: coexistence of Dirac and Weyl fermions in polar hexagonal ABC crystals[J]. Physical Review Letters, 2018, 121(10): 106404.

[13] Ma J, Yi C, Lv B, et al. Experimental evidence of hourglass fermion in the candidate nonsymmorphic topological insulator KHgSb[J]. Science Advances, 2017, 3(5): e1602415.

[14] Kuo C S, Chang T R, Xu S Y, et al. Unconventional topological phase transition in non-symmorphic material KHgX (X = As, Sb, Bi) [J]. npj Computational Materials, 2019, 5: 65.

[15] Song J, Kim S, Kim Y, et al. Coexistence of surface superconducting and three-dimensional topological Dirac states in semimetal KZnBi[J]. Physical Review X, 2021, 11(2): 021065.

[16] Zhou Z, Peng K, Xiao S, et al. Anomalous thermoelectric performance in asymmetric Dirac semimetal BaAgBi[J]. The Journal of Physical Chemistry Letters, 2022, 13(10): 2291-2298.

[17] Xu S, Wang H, Wang Y Y, et al. Crystal growth of BaAgAs family topological materials via flux method[J]. Journal of Crystal Growth, 2020, 531: 125304.

[18] Ma T C, Hu J N, Chen Y, et al. Coexistence of type-II and type-IV Dirac fermions in SrAgBi[J]. Modern Physics Letters B, 2021, 35(19): 2150181.

最新录用，非最终出版稿

[19] Lee N, Pei C, Koo J, et al. Pressure-dependent superconductivity in topological Dirac semimetal SrCuBi[J]. Advanced Materials, 2024, 36: 2400428.

[20] Cheng E, Xia W, Shi X, et al. Pressure-induced superconductivity and topological phase transitions in the topological nodal-line semimetal $SrAs_3$[J]. npj Quantum Materials, 2020, 5: 38.

[21] Jin M, Yu P, Fan C, et al. Discovery of dome-shaped superconducting phase and anisotropic transport in a van der Waals layered candidate $NbIrTe_4$ under pressure[J]. Advanced Science, 2021, 8: 2103250.

[22] He L, Jia Y, Zhang S, et al. Pressure-induced superconductivity in the three-dimensional topological Dirac semimetal Cd_3As_2[J]. npj Quantum Materials, 2016, 1: 16014.

[23] Mao H K, Xu J, Bell P M. Calibration of the ruby pressure gauge to 800 kbar under quasi-hydrostatic conditions[J]. Journal of Geophysical Research, 1986, 91(B5): 4673-4676.

[24] Zhao Y, Clément S, Haines J, et al. Lattice dynamics study of elemental bismuth under high pressure[J]. The Journal of Physical Chemistry C, 2020, 124(48): 26659-26669.

[25] Zhu, Yinghao, et al. Superconductivity in pressurized trilayer $La_4Ni_3O_{10-\delta}$ single crystals. *Nature* 2024, 8021(631): 531-536.

[26] Li Y, Wang E, Zhu X, et al. Pressure-induced superconductivity in Bi single crystals[J]. Physical Review B, 2017, 95(2): 024510.

[27] Zhang Y, Gouchi J, Ishigaki K, et al. Abnormal transport properties of Bi-III superconducting phase in pressurized bismuth single crystal[J]. Superconductor Science and Technology, 2021, 34(7): 075009.

[28] Woollam J A, Somoano R B, O'Connor P. Positive curvature of the H_{c2} versus T_c boundaries in layered superconductors[J]. Physical Review Letters, 1974, 32(13): 712-714.

[29] Clogston A M. Upper limit for the critical field in hard superconductors[J]. Physical Review Letters, 1962, 9(6): 266-267.

[30] Chen X, Shao D, Gu C, et al. Pressure-induced multiband superconductivity in pyrite $PtBi_2$ with perfect electron-hole compensation[J]. Physical Review Materials, 2018, 2(5): 054203.

[31] Chen X, Shao D, Gu C, et al. Pressure-induced superconductivity in trigonal layered $PtBi_2$ with triply degenerate point fermions[J]. Physical Review B, 2021, 103(1): 014507.

[32] Song J, Park B C, Sim K I, et al. Tunable Berry curvature and transport crossover in topological Dirac semimetal KZnBi[J]. npj Quantum Materials, 2021, 6: 77.

[33] Abrikosov A A. Quantum magnetoresistance[J]. Physical Review B, 1998, 58(5): 2788-2794.

[34] Murakawa H, Bahramy M S, Tokunaga M, et al. Detection of Berry's phase in a bulk Rashba semiconductor[J]. Science, 2013, 342(6165): 1490-1493.

[35] Zhao Y, Liu H, Zhang C, et al. Anisotropic Fermi surface and quantum limit transport in high mobility three-dimensional Dirac semimetal Cd_3As_2[J]. Physical Review X, 2015, 5(3): 031037.

[36] Bardeen J, Cooper L N, Schrieffer J R. Microscopic theory of superconductivity[J]. Physical Review, 1957, 106(1): 162-164.

[37] McMillan W L. Transition temperature of strong-coupled superconductors[J]. Physical Review, 1968, 167(2): 331-344.

录用稿件，非最终出版稿

[38] Lv X D, Li S M, Huang Y P, et al. Interplay of structure and superconductivity in α-SnS tuned by pressure[J]. Physical Review B, 2024, 110(5): 054107.

[39] Xu S, Yang P, Chen K, et al. Superconducting phase diagram and the evolution of electronic structure across charge density wave in underdoped 1T-CuxTiSe$_2$ under hydrostatic pressure[J]. Physical Review B, 2021, 104(13): 134503.

[40] Lifshitz I M. Anomalies of electron characteristics of a metal in the high pressure region[J]. Soviet Physics JETP, 1960, 11(5): 1130-1135.

[41] Liu F L, Li J H, Zhang K N, et al. Pressure-induced Lifshitz transition in the type II Dirac semimetal PtTe$_2$[J]. Science China Physics, Mechanics & Astronomy, 2019, 62(4): 048211.

[42] Dai G Y, Zheng Q F, Hao Z Y, et al. Pressure effect on the electrical properties and pressure-induced phase transitions in a three-dimensional Dirac semimetal BaAgBi[J]. Physica B: Condensed Matter, 2023, 666: 415086.

[43] Langmann E. Ubiquity of superconducting domes in the Bardeen–Cooper–Schrieffer theory with finite-range potentials[J]. Physical Review Letters, 2019, 122(15): 157001.

[44] Boudjada N, Buessen F L, Paramekanti A. Domes of T_c in single-band and multiband superconductors with finite-range attractive interactions[J]. Physical Review B, 2020, 102(5): 054504.

Appendix

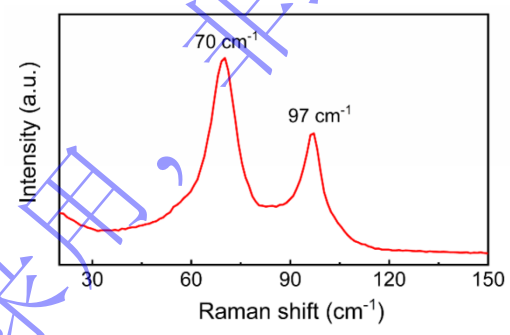
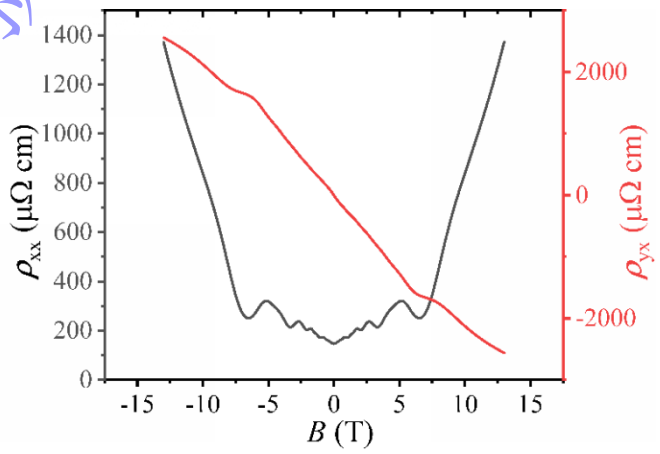


FIG. S1. Raman spectra of KZnBi at ambine pressure.



最新录用，非最终出版稿

FIG. S2. Longitudinal resistance (ρ_{xx}) and Hall resistance (ρ_{xy}) of KZnBi as a function of the perpendicular magnetic field (B) applied along the c-axis (perpendicular to the current plane).

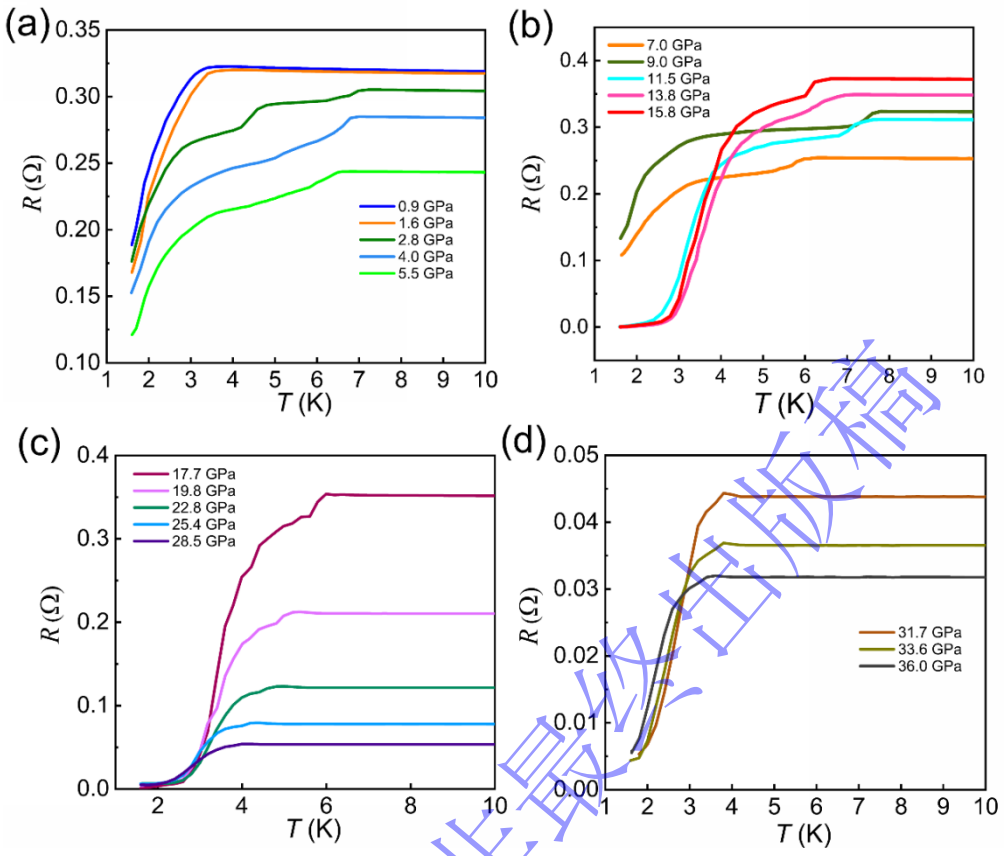


FIG. S3. (a)–(d) Close-up views of low-temperature resistance data ($0 \le T \le 10$ K) for KZnBi at various pressures.

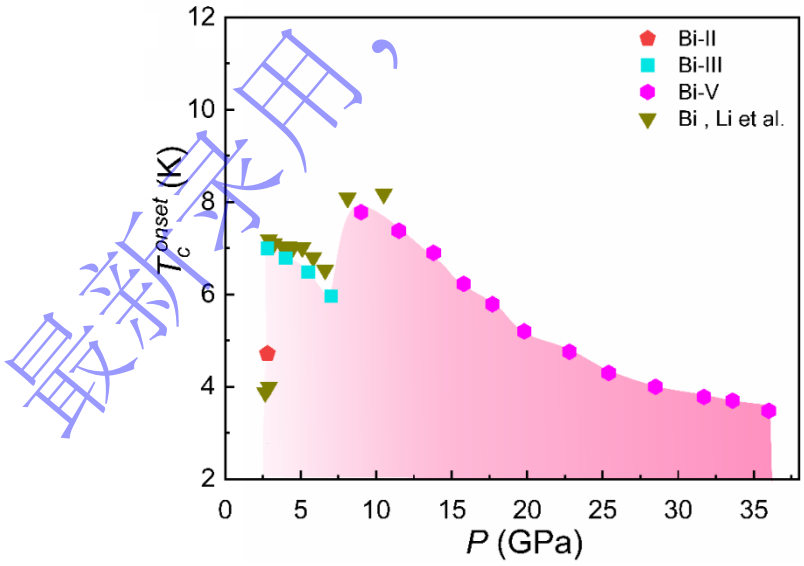


FIG. S4. Temperature-pressure (T-P) phase diagram of bismuth, compared with results from Li *et al.*.[26,27]

非最终出版稿
最新录用，

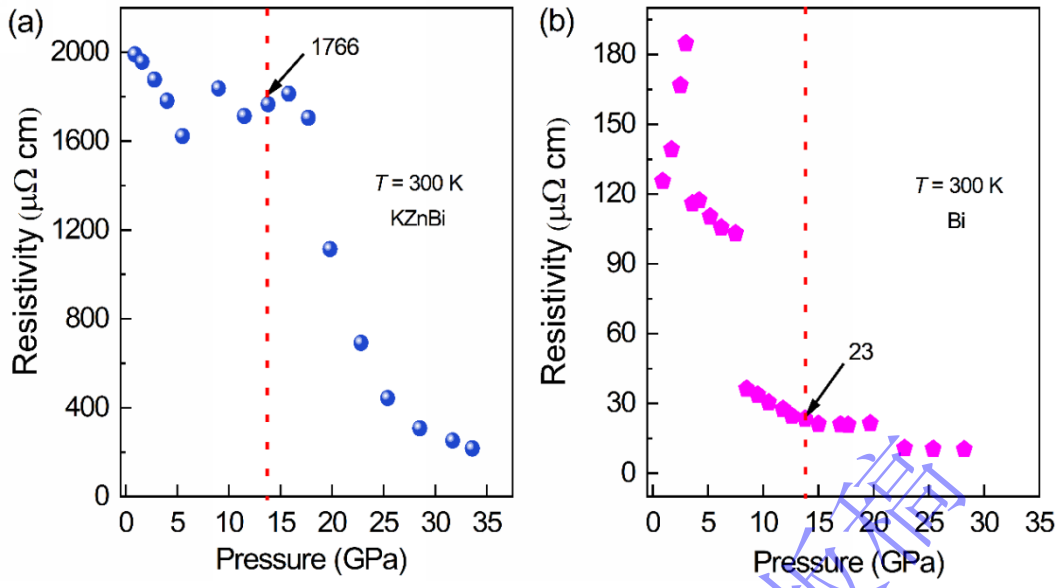


FIG. S5. (a) Pressure dependence of resistivity of a KZnBi single crystal at 300 K. (b) Variation of resistivity with pressure for a Bi single crystal at 300 K.

At 0.9 GPa, the resistivity of KZnBi is ~1990 μΩ·cm [Fig. S5(a)], a value consistent with that reported for KZnBi.[15] This indicates that the dominant charge transport originates from the KZnBi matrix. Moreover, the resistivity of KZnBi at this pressure exceeds that of single-crystal Bi by more than a factor of 15 [Fig. S5(b)]. The magnitude and pressure dependence of the Bi resistivity obtained here agree well with previous reports,[4,5] confirming the reliability of our comparative data and underscoring the pronounced resistivity contrast between KZnBi and Bi.

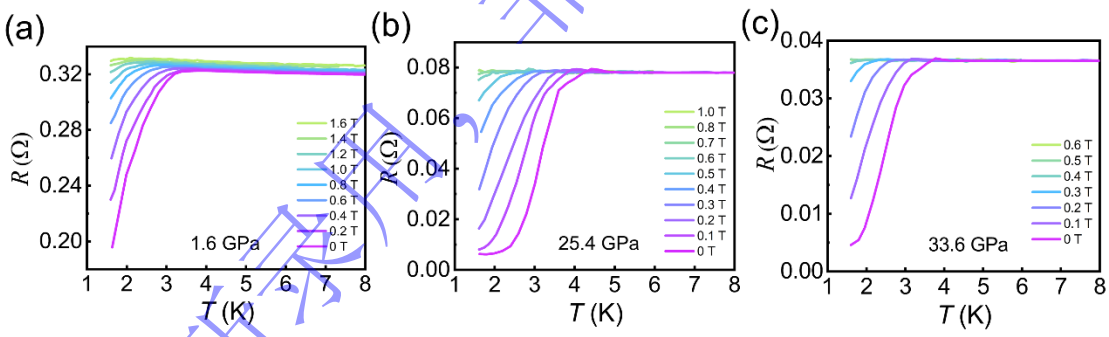


FIG. S6. (a-d) Field dependences of electrical resistance for KZnBi at 1.6 GPa (a), 25.4 GPa (b) and 33.6 GPa (c).

录用稿件，非最终出版稿

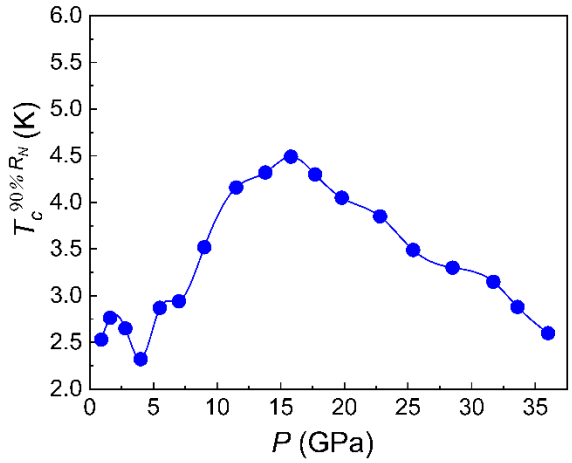


FIG. S7. Temperature–pressure phase diagram of KZnBi, plotted as $T_c^{90\%R_N}$ versus P. Here $T_c^{90\%R_N}$ is defined as the temperature at which the resistivity drops to 90% of the normal-state resistance R_N.

最终录用，非最终出版稿

拓扑狄拉克半金属 KZnBi 中压力诱导的穹顶状超导性

郑群飞[1]，赵凌霄[1,2]，童浩轩[1]，程文静[1]，李辰恺[1]，刘净宜[1]，陈吴昊[2]，刘影[2,3]，朱金龙[1, 2, 3*]

（1.南方科技大学物理系，量子功能材料全国重点实验室，广东省高等学校量子科学基础研究卓越中心，广东 深圳 518055；
2.粤港澳大湾区（广东）量子科学中心，广东 深圳 518045;
3.南方科技大学新材料重大科学设施研究院，广东 深圳 518055）

摘 要：三维拓扑狄拉克半金属 KZnBi 具有对称性保护的狄拉克费米子，并在常压下表现出超导性，为研究拓扑态与超导性之间的相互作用提供了较为吸引力的体系。报道了 KZnBi 在高达 36 GPa 压力下变温电阻、横向磁阻和霍尔电阻的测量结果。超导起始转变温度T_c^{onset}随压力呈非单调变化。第一个穹顶约在 0.9 GPa 开始形成，T_c^{onset}在约 1.6 GPa 达到最大值，随后在约 4.0 GPa 附近降至最小值。继续加压后，T_c^{onset}再次升高，并在 15.8 GPa 附近形成第二个穹顶，其最大值约为 4.2 K。这些结果构建了 KZnBi 丰富的温度–压力相图，并表明其超导行为与电子结构密切相关。

关键词：高压；拓扑狄拉克半金属；超导性；超导转变温度；霍尔电阻

Keywords：high pressure; topological dirac semimetal; superconductivity.